

**1 Implications of representing snowpack stratigraphy**  
**2 for large-scale passive microwave remote sensing**

Konstantinos M. Andreadis

**3** Civil and Environmental Engineering, University of Washington, Seattle, WA

Dennis P. Lettenmaier

**4** Civil and Environmental Engineering, University of Washington, Seattle, WA

---

K. M. Andreadis, Department of Civil and Environmental Engineering, University of Washington, Wilson Ceramic Lab, Box 352700, Seattle, WA 98195, USA. (kostas@hydro.washington.edu)

5 **Abstract.** The layered character of snowpacks increases the complexity  
6 of algorithms intended to retrieve snow properties, such as water equivalent,  
7 from the snowpack microwave return signal. However, it also offers the op-  
8 portunity to infer snowpack microphysical properties by combining differ-  
9 ent frequencies and polarizations, and therefore has the potential for fully  
10 self-consistent retrieval algorithms applicable to multi-frequency sensors, which  
11 avoids the necessity for additional information sources which are otherwise  
12 required. Implementation of a multifrequency snow property retrieval strat-  
13 egy requires knowledge of the stratigraphy of snowpack microphysical prop-  
14 erties, which as a practical matter can only be produced by predictive (for-  
15 ward) models that include representation of spatial variability of vegetation  
16 and snow characteristics. We describe a multi-layer snow model designed for  
17 such applications. The model is computationally efficient to the extent that  
18 it can be implemented at the scale of large watersheds, or even over conti-  
19 nents. The models ability to replicate large-scale snowpack layer features is  
20 evaluated using observations from the Cold Land Processes Experiment (CLPX)  
21 and a 2002 Nome-Barrow snowpit transect (SnowSTAR 2002). The multi-  
22 layer model coupled with a radiative transfer scheme improved the estima-  
23 tion of brightness temperatures both in terms of absolute values and frequency/polarization  
24 differences (error reductions ranging from 47 to 72%). The effects of certain  
25 stratigraphic features on large-scale microwave emissions are demonstrated,  
26 while potential impacts of using a multi- versus a single-layer model when  
27 assimilating radiances are explored.

## 1. Introduction

28 Snow is a key component of the global hydrologic cycle, especially in mid to high  
29 latitudes. From a hydrological standpoint, snowpacks act as storage reservoirs which  
30 modulate the seasonal cycle of runoff. The space-time distribution of snow can also affect  
31 atmospheric processes as a result of the strong contrast in albedo and surface temperature  
32 between snow covered and snow free surfaces. These contrasts can alter atmospheric  
33 circulation patterns [*Heim and Dewey, 1984; Cohen and Entekhabi, 1999*]. The spatial  
34 and temporal sparseness of in-situ observation networks globally have led to reliance on  
35 remotely sensed observations of snow properties, especially snow cover extent, at large  
36 scales [*Schmugge et al., 2002*]. However, the production of consistent, accurate satellite-  
37 based estimates of snow water equivalent, the key hydrological variable associated with  
38 snow, remains elusive.

39 Satellite observations of snow properties have been available for more than 40 years,  
40 mostly based on visible and passive microwave sensors. Although visible wavelength sen-  
41 sors provide a basis for estimating snow cover extent, they do not provide any information  
42 about snow water storage, which is hydrologically more important. Passive microwave re-  
43 mote sensing has been used to operationally map snow cover and depth since 1978 [*Chang*  
44 *et al., 1987; Kelly et al., 2003*], however its use is generally limited to relatively thin,  
45 cold snowpacks. Previous studies have shown correlations between passive microwave  
46 brightness temperatures and snow depth [e.g. *Künzi et al., 1982; Hallikainen and Jolma,*  
47 *1992; Josberger and Mognard, 2002; Derksen et al., 2003*], but many limitations neverthe-  
48 less make direct retrieval of snow properties from passive microwave sensors problematic

49 [*Dong et al.*, 2005; *Foster et al.*, 2005; *Derksen et al.*, 2005]. These problems include the  
50 coarse spatial resolution of current sensors, signal “saturation” (related to the penetration  
51 depth for different frequencies), presence of liquid water in the snowpack which dimin-  
52 ishes volume scattering and hence limits retrieval algorithms, dense forest cover (which  
53 dominates the microwave signal), as well as snow metamorphism which can strongly alter  
54 microwave emissivity and thus complicates retrieval algorithms.

55 The experience to date is that satellite observations alone cannot provide a means for  
56 estimating snow water storage at large scales, aside from a few highly specific cases.  
57 An alternative approach is to merge remotely sensed observations with physically-based  
58 model predictions to constrain retrieval algorithms and potentially account for the uncer-  
59 tainties (e.g. through data assimilation [*Durand and Margulis*, 2006; *Pulliainen*, 2006]).  
60 Such an approach would require coupling a large-scale snow hydrology and a microwave  
61 emission model. Although there have been a few studies [*Andreadis et al.*, 2008a; *Du-*  
62 *rand et al.*, 2008] that have evaluated microwave brightness temperatures predicted by  
63 such coupled models, a key issue is that a discrepancy exists between the assumption of  
64 homogeneous snowpacks inherent in most land surface models and the fact that snow is  
65 a naturally layered medium [*Andreadis et al.*, 2008a]. Moreover, anomalous behavior of  
66 microwave emissivity, such as increasing brightness temperatures with increasing snow  
67 depth, is sometimes observed from satellite and ground measurements [*Rosenfeld and*  
68 *Grody*, 2000a], and can be attributed to snow metamorphic processes and the snowpack  
69 layering structure [*Hofer and Mätzler*, 1980; *Rosenfeld and Grody*, 2000b]. In cases when  
70 the wavelength is comparable to either layer thicknesses or particle sizes, and when there  
71 are sufficient differences in the dielectric properties between layers, microwave signals can

72 be very different for otherwise comparable snowpacks [Colbeck, 1991]. For example, the  
73 presence of an ice layer within a snowpack can change its brightness temperature by up  
74 to 50 K [Edgerton et al., 1971], while depth hoar can significantly decrease brightness  
75 temperature by increasing scattering due to its prevailing larger snow crystals [Hall et al.,  
76 1986].

77 The layered character of snowpacks increases the difficulties in deconvolving the return  
78 microwave signal (passive or active), but it also offers the opportunity to infer the meta-  
79 morphic signature of the observed snowpack [Rosenfeld and Grody, 2000b] and to extract  
80 snowpack microphysical information by combining different frequencies and polarizations.  
81 In order to exploit this potential, snowpack stratigraphic information is required. Given  
82 the spatial scales supported by existing satellite technology, this prior information can  
83 only be provided by snow models applicable to the spatial scale of passive microwave  
84 sensors (typically tens of km) that can represent layered snowpacks. Key questions then  
85 become how to capture the spatial variability of snow layering in a forward model, and  
86 how that variability is reflected in the satellite microwave signal.

87 Snowpack layering is affected by meteorological (wind, air temperature, precipitation,  
88 solar radiation) as well as topographic (slope, aspect) and physiographic (presence or ab-  
89 sence of vegetation) controls. Sturm and Benson [2004] examined the spatial heterogeneity  
90 of snowpack stratigraphy over distances ranging from 10 m to more than 200 km using  
91 snowpit measurements collected on the Arctic coastal plain of Alaska. They found that  
92 at scales greater than 100 m, topographic variations can result in substantial variations  
93 in precipitation, wind, and solar radiation which in turn are reflected in heterogeneity in  
94 snowpack stratigraphy, while such variations can also be caused by snow-vegetation in-

95 teractions [*Sturm*, 1992]. However, notwithstanding these small scale variations, at scales  
96 larger than about 10 km, there was a general coherence in the snowpack layers which had  
97 relatively strong spatial correlations across the Kuparuk basin [*Sturm and Benson*, 2004]  
98 for distances ranging from 10-25 km. Weather appeared to be the primary driver for this  
99 synoptic-scale variability that led to snow layers remaining recognizable over distances  
100 order of 160 km, notwithstanding that the landscape and its interactions with weather in-  
101 troduced relatively smaller-scale heterogeneity that distorted the larger-scale trends. The  
102 combined effects of controls at these two scales was noted by *Schweizer and Kronholm*  
103 [2007], who observed a layer of surface hoar over an approximately 250 km<sup>2</sup> area, the  
104 spatial coherence of which was eventually reduced by local effects of wind and aspect  
105 variability.

106 The objective of this study is to develop a macroscale multilayer snow model that can  
107 reflect spatial variability in the controlling processes at multiple scales, and can replicate  
108 large-scale snowpack layer features and their effect on passive microwave emissivity. Such  
109 a model, which would account for sub-grid variability in topography and land cover and  
110 their interactions with precipitation, air temperature and wind would potentially be able  
111 to capture the large-scale layering features that would affect satellite retrievals, such as  
112 surface and depth hoar, by simulating snowpack physics within these relatively homoge-  
113 neous areas. The model we have developed with this objective in mind is described in the  
114 following section. Section 3 presents the model validation results. Validation is performed  
115 both in terms of snow stratigraphy and microwave emissivity, while this study also exam-  
116 ines the effects of certain stratigraphic features on the satellite-scale observations, as well

117 as present a comparison of the potential use of a multi-layer versus a single-layer forward  
118 model to assimilate satellite passive microwave observations.

## 2. Model description

119 The multi-layer snowpack model is based on a mass and energy balance. We describe  
120 the foundations for the model below along with a brief description of the overall model  
121 structure in a macroscale setting.

### 2.1. General model structure

122 Many snowpack models have been developed for different applications including hydro-  
123 logical prediction, global circulation modeling, and avalanche forecasting [*Etchevers et al.*,  
124 2004]. These models vary in complexity, ranging from simple force-restore schemes [*Yang*  
125 *et al.*, 1997], to approaches assuming snowpacks as homogeneous media [*Verseghy*, 1991;  
126 *Wigmosta et al.*, 1994; *Koren et al.*, 1999], to multi-layered representations with detailed  
127 snowpack physics [*Brun et al.*, 1989; *Jordan*, 1991; *Bartelt and Lehning*, 2002]. Given our  
128 objectives, a physically-based representation of snowpack internal processes is required  
129 that would be of intermediate complexity and efficient enough to simulate stratigraphy  
130 over large scales, [e.g. *Loth et al.*, 1993; *Sun et al.*, 1999]. Our approach here is similar  
131 to previous studies, adapting existing models [*Jin et al.*, 1999] and coupling them to a  
132 large-scale model [*Boone and Etchevers*, 2001].

133 The macroscale model, which provides a framework for our development, is the Variable  
134 Infiltration Capacity (VIC) model [*Liang et al.*, 1994], which solves the water and energy  
135 balance of a soil column over a gridded domain accounting for sub-grid variability in land  
136 cover by partitioning each model grid cell into tiles based on topography and land cover.

137 Spatial heterogeneity in runoff generating processes is represented by a parameterization  
 138 of the combined effects of topographic and small scale spatial variability in soil proper-  
 139 ties. Water and energy states and fluxes are simulated for each “homogeneous” tile and  
 140 averaged over each model grid cell. The multi-layer snowpack model we develop here  
 141 is intended to be coupled to VIC in such a way as to retain the interactivity between  
 142 the current essentially single-layer snowpack model and other components including the  
 143 canopy snow interception and energetics [Andreadis et al., 2008b], frozen soils [Cherkauer  
 144 and Lettenmaier, 2003], and blowing snow [Bowling et al., 2004] sub-models.

## 2.2. Energy balance

The snowpack is represented as a layered medium, with energy exchange between snow and the atmosphere limited to the surface layer taking the form

$$Q^* = (1 - \alpha)Q_s \downarrow + Q_l \downarrow - Q_l \uparrow + Q_h + Q_e + Q_a - Q_c - Q_{lw} - \Delta H \quad (1)$$

145 where  $Q_s \downarrow$  is the downward shortwave radiation,  $\alpha$  is the snow albedo,  $Q_l \downarrow$  is the  
 146 downward longwave radiation,  $Q_l \uparrow$  is the emitted longwave radiation ( $= \epsilon \sigma T_{s,t}^4$ ) where  $\epsilon$  is  
 147 the emissivity,  $\sigma$  is the Stefan-Boltzmann constant and  $T_s$  is the snow surface temperature,  
 148  $Q_h$  is the sensible heat flux (including advected sensible heat flux),  $Q_e$  is the latent heat  
 149 flux (including heat flux from sublimation),  $Q_a$  is the advected heat from rainfall,  $Q_c$   
 150 is the heat conducted to/from the deeper snowpack,  $Q_{lw}$  is the heat associated with  
 151 liquid water percolation,  $\Delta H$  is the change in heat content  $\left( = c_i h_m \frac{T_t - T_{t-1}}{\Delta t} \right)$  where  
 152  $c_i$  is the heat capacity of ice,  $h_m$  is the snow water equivalent, and  $T_t$ ,  $T_{t-1}$  are the  
 153 temperatures at the current and previous time steps respectively, and  $Q^*$  is the energy  
 154 available for melting or refreezing. Albedo is calculated as a function of snow age using an

155 empirical relationship [Andreadis et al., 2008b], while incoming shortwave and longwave  
 156 radiations are provided either from measurements or can be estimated [Thornton and  
 157 Running, 1999]. Turbulent heat fluxes and advected energy from rainfall are calculated  
 158 using the formulations in Wigmosta et al. [1994] depending on atmospheric pressure, air  
 159 temperature, rainfall amount, and saturation vapor pressure and temperature at the snow  
 160 surface.

Heat conduction through the snowpack is modeled as

$$Q_{c,j} = k_j \frac{\partial T}{\partial z} \quad (2)$$

where  $k_j$  is the heat conductivity, and  $\frac{\partial T}{\partial z}$  is the temperature gradient across layer  $j$  (if  
 this layer is the bottom layer,  $Q_c$  becomes the ground heat flux). Heat conductivity can be  
 estimated in a number of ways; here, it is calculated from a quadratic relationship between  
 conductivity and density derived from a measurement data set that encompassed most  
 types of seasonal snow cover [Sturm et al., 1997]. The energy balance for the internal  
 layers can be formulated as

$$Q_j^* = Q_{s,j} - Q_{lw,j-1} + Q_{lw,j} - Q_{c,j-1} + Q_{c,j} - Q_{h,j-1} + Q_{h,j} - \Delta H_j \quad (3)$$

161 where  $Q_{s,j}$  is the shortwave radiation penetrating to this layer,  $Q_{lw,j}$  is the energy associ-  
 162 ated with water movement from layer  $j$  to  $j+1$   $\left( = c_w \frac{U_{l,j} T_j}{\Delta t} \right)$  and  $c_w$  is the heat capacity  
 163 of water and  $U_{l,j}$  the liquid water flux from layer  $j$ ,  $Q_{c,j}$  is heat conducted from layer  $j$   
 164 to  $j+1$ , and  $Q_{h,j}$  is the latent heat released from vapor diffusion from layer  $j$  to  $j+1$   
 165  $\left( = L_s \frac{U_{v,j} \rho_w}{\Delta t} \right)$  with  $L_s$  being the latent heat of sublimation,  $U_{v,j}$  the vapor flux from  
 166 layer  $j$ , and  $\rho_w$  the water density. The energy balance is solved as a system of equations

167 using the iterative discrete Newton algorithm [*Dennis and Schnable*, 1983], or as an Euler  
 168 backward tridiagonal system if the first method does not converge [*Loth et al.*, 1993].

### 2.3. Mass balance

After solving for the snowpack temperature profile, the amounts of water that have melted or refrozen are calculated and liquid water is allowed to percolate from one layer to another using a 35% retention capacity. Along with the liquid water flux, vapor fluxes are calculated from the Clausius-Clapeyron equation

$$U_v = -D_s \frac{p_s}{RT^2} \left( \frac{L_s}{RT} - 1 \right) \frac{\partial T}{\partial z} \quad (4)$$

169 where  $p_s$  is the vapor saturation pressure,  $R$  is the water vapor gas constant, and  $D_s$  is  
 170 the vapor diffusion coefficient for snow estimated from *Colbeck* [1993].

171 Two important processes related to snow metamorphism are densification and grain  
 172 growth. The former is caused by compaction of snow layers, destructive (equi-  
 173 temperature), constructive (temperature gradient), and melt metamorphism. *Anderson*  
 174 [1976] developed a model for snow densification taking these processes into account, which  
 175 has been adapted to the VIC model with the essentially single-layer formulation [*Andreadis*  
 176 *et al.*, 2008b], and has been extended to the multi-layer version by calculating snow den-  
 177 sity changes for each layer. The snow grain growth model is adapted from *Lehning et al.*  
 178 [2002], and uses empirical relationships for equilibrium growth metamorphism (small tem-  
 179 perature gradients, less than 5 K), and wet snow metamorphism (presence of liquid water  
 180 in the snowpack) [*Brun*, 1989]. When temperature gradients are larger than 5 K, higher  
 181 growth rates occur (kinetic growth metamorphism) and both layer-to-layer and intra-layer  
 182 vapor transport contribute to the water vapor supply [*Sturm and Benson*, 1997].

183 The snow model is formulated in a way such as to be computationally feasible for  
184 simulating snowpacks across large scales. Therefore, some constraints are required in the  
185 combination of layers to keep the number of layers below a prescribed maximum. A new  
186 layer is created after every snowfall event as long as it has a snow water equivalent of 5 mm,  
187 while the surface layer snow mass is not allowed to exceed 20 mm. At the end of each time  
188 step, two neighboring layers are combined if both are cold and their temperature gradient  
189 is less than 5 K/m. When the maximum number of layers is exceeded by invoking these  
190 criteria, the two layers with the minimum temperature gradient and density difference are  
191 combined.

### 3. Results

#### 3.1. Cold Land Processes Experiment, Colorado

192 The Cold Land Processes Experiment (CLPX) was a multi-sensor and multi-scale field  
193 campaign conducted during the winters of 2002 and 2003 over a set of nested areas in  
194 Colorado and Wyoming. A set of snowpit detailed measurements were taken in a  $100 \times 100$   
195 m clearing, designated as the Local Scale Observation Site (LSOS), in addition to radio-  
196 metric measurements from a Ground-Based Microwave Radiometer (GBMR-7). Snowpit  
197 measurements included snow depth, water equivalent, density, temperature and grain size  
198 profiles which were collected between November 2002 and March 2003, while the GBMR-7  
199 measurements included brightness temperatures at 18.7, 23.8, 36.5 and 89 GHz during  
200 selected days in January and December 2002 and February and March 2003 [*Graf et al.*,  
201 2003].

202 This set of measurements offered an opportunity to simultaneously test the ability  
203 of VIC to reproduce stratigraphic profiles, and to simulate the corresponding passive

204 microwave response after being coupled with a radiative transfer model. The model was  
205 allowed to have a maximum number of five layers, and was forced with daily precipitation,  
206 maximum, minimum air temperature and wind speed in a manner similar to [Maurer  
207 *et al.*, 2002]. This was done to emulate the general data availability and computational  
208 feasibility when applying such macroscale hydrological models in off-line settings. The  
209 simulation period was from 1 October 2002 (no snow) to 25 March 2003. The model  
210 used internal algorithms to disaggregate the daily meteorological data (by partitioning  
211 precipitation into equal-magnitude increments with diurnal variability introduced to air  
212 temperature) and/or to calculate required inputs at the model time step (in the case  
213 of relative humidity, incoming shortwave and longwave radiation) as outlined in Maurer  
214 *et al.* [2002].

### 215 **3.1.1. Snowpack stratigraphy**

216 Before examining how well snowpack stratigraphy is simulated by the multilayer model,  
217 it is important to evaluate the accuracy of the model in simulating snow water equivalent.  
218 Fig. 1 shows the simulated snow water equivalent (SWE) for both the 5-layer and standard  
219 (surface and pack layer) VIC snow models compared with snow pit measurements. Both  
220 model simulations are quite close to the observed SWE, although they seem to slightly  
221 underestimate snow accumulation in March 2003. The differences in simulated snow mass  
222 between the two model versions are minimal, with the single- and multi-layer relative  
223 having mean squared errors of 9.4 mm (6.1%) and 11.7 mm (7.3%) respectively. The  
224 differences are mostly attributable to small differences in sublimation rates.

225 Fig. 2 shows a representative set of simulated and observed snow temperature, density  
226 and grain size profiles for selected dates (22 January, 2 and 20 February, and 11 March

2003) at the LSOS site. The model appears to be able to simulate snowpack temperature quite well, with small discrepancies occurring either because of underestimated incoming shortwave radiation (Fig. 2b) or underestimated snow depth (Fig. 2c). The model predicts a colder temperature than observed at the middle of the snowpack for the March 11 pit (Fig. 2d), although the surface, top 20 cm and ground temperatures are predicted correctly. Results are similar for snow density, the model reproduces the density profile quite accurately for the January snowpit (Fig. 2a) but underestimates the densification rate for the upper portion of the pack during February (Fig. 2b,c). When partial melting occurs during March, the model predicts a larger density gradient while the observations show a more gradual change in density with depth (Fig. 2d). However, the model does capture the qualitative features of the increase in density near the surface and the decrease in the deeper layers. Evaluation of the predicted grain size is difficult because of the range in the measurements, and the single model value for each layer. Fig. 2a shows that the model underestimates grain size for the deeper layers, but predicts it quite well for the upper layers. During February (Fig. 2b,c) the model is able to predict the large near-surface grain size, as well as the bottom depth hoar evident in the measurements. Simulated grain size is relatively close to the observed range in the March snowpit (Fig. 2d) as well, with a small underestimation near the snowpack mid-depth.

### 3.1.2. Ground-based microwave brightness temperatures

Potential improvements in microwave emission model predictions when using a multiple layer coupled (hydrologic and radiative transfer) model over a single-layer one were assessed using the GBMR-7 measurements. The latter were taken on selected dates in February 2003 within the LSOS site and included measurements of brightness tempera-

250 ture at 18.7, 23.0, 36.5 and 89.0 GHz. The microwave emission model used is based on  
251 the Dense Media Radiative Transfer (DMRT) theory and quasi-crystalline approximation  
252 [*Tsang et al.*, 1985, 2000]. The model does not make the assumption of independent scat-  
253 tering, and takes into account inter-particle forces that lead to adhesion and collective  
254 scattering calculating microwave emissivity as a function of snow depth, density, grain  
255 size and temperature [*Tsang et al.*, 2007]. The degree of particle clustering is modeled  
256 through a stickiness parameter, which also affects the frequency dependence of the ex-  
257 tinction coefficient. Recently, the DMRT was extended to a multi-layer formulation, and  
258 was shown to agree very well with the GBMR-7 ground measurements when forced with  
259 observed snow stratigraphy [*Liang et al.*, 2008]. Here, we used the VIC multilayer snow  
260 model stratigraphy in place of observations for DMRT, with the stickiness parameter was  
261 set to the default value of 0.1 for all snowpack layers.

262 Fig. 3 compares the single and multiple layer simulations of brightness temperatures  
263 with the GBMR-7 measurements at 18.7 GHz (Fig. 3a) and 36.5 GHz (Fig. 3b) at both  
264 horizontal and vertical polarizations. The improvement in predicting 18.7 GHz TB using  
265 5 layers is evident for all measurement dates except 2/19 for the vertical and 2/20 for  
266 both polarizations. Similarly, for 36.5 GHz the 5-layer model better predicted TB with  
267 the exception of 2/21 for the horizontal and 2/22 for the vertical polarization. The cor-  
268 responding prediction root mean squared errors (RMSE) for the four frequency channels  
269 (18.7 GHz horizontal and vertical, and 36.5 GHz horizontal and vertical) were 14.0, 5.5,  
270 13.3, 9.4 K for the single-layer coupled model, and 5.5, 2.9, 5.2, 3.4 K for the 5-layer  
271 VIC/DMRT model. These results appear to confirm the hypothesis in previous work  
272 using the single-layer VIC/DMRT [*Andreadis et al.*, 2008a], that predictions of TB for

273 horizontal polarizations were problematic because of the reflection at layer boundaries,  
274 which was not captured by the single-layer model and mostly affects horizontal polariza-  
275 tion [*Wiesmann and Mätzler, 1999*].

276 The 5-layer coupled model is also able to reproduce the observed frequency and polar-  
277 ization differences in the LSOS site better than the single layer model (Fig. 4). The errors  
278 in predicting polarization differences (in terms of RMSE) for the 1-layer model were 9.8  
279 and 8.7 K for 18.7 and 36.5 GHz, which were reduced by the 5-layer model to 3.9 and 3.3  
280 K respectively. The error reduction is also evident in the scatter plot in Fig. 4a, which  
281 shows simulated versus observed polarization differences. Fig. 4b shows simulated versus  
282 observed frequency differences for both 1-layer and 5-layer models and both polarizations.  
283 The 1-layer model has similar frequency difference prediction errors for both polarizations,  
284 11.9 and 11.4 K for the horizontal and vertical, while the 5-layer model decreases those  
285 errors to 9.1 and 5.6 K respectively.

### 3.2. SnowSTAR 2002 Transect, Alaska

286 A series of snowpack stratigraphy measurements (designated SnowSTAR 2002) were  
287 taken in arctic Alaska along a transect extending 750 km from Nome to Barrow, AK  
288 during March and April 2002 [*Sturm and Liston, 2003; Sturm and Benson, 2004*]. These  
289 measurements span distances that range from 10 m to 200 km between snowpits, and  
290 include snow depth, density, grain size, temperature, water equivalent, hardness, type,  
291 and fractions of wet, recent snow, slabs, and hoar. The prevalent land cover along the  
292 traverse is tundra, while the area is fairly flat with relatively low relief and most elevations  
293 being below 500 m. These data the opportunity to evaluate the relationship between large-

294 scale variability in stratigraphy and satellite-observed passive microwave emissions, given  
295 the relative homogeneity and absence of dense forest cover.

296 Satellite observations of microwave brightness temperature, taken from the Special Sen-  
297 sor Microwave Imager (SSM/I) [*Grody and Basist, 1996*], were used to examine the change  
298 in microwave emissivity with snow depth. Fig. 5 shows snow depth measurements from  
299 different dates for each co-registered SSM/I 25×25 km pixel and the corresponding bright-  
300 ness temperatures for 37 GHz, which is probably the most appropriate frequency given  
301 snowpack depths and the typical penetration depths for passive microwave frequencies.  
302 Satellite pixels which contained lakes were excluded to isolate the effects of snowpack  
303 variability on brightness temperatures [*Duguay et al., 2005*], while both polarizations  
304 (horizontal and vertical) and orbits (ascending and descending) are shown for the SSM/I  
305 observations. Although there is a general pattern of increasing (decreasing) brightness  
306 temperature with decreasing (increasing) snow depth across the transect, there are clearly  
307 cases where the opposite is true. Possible reasons for this behavior include the effects of  
308 different snowpack stratigraphy as well as the potential spatial variability within each  
309 satellite pixel. We examine below two particular cases to demonstrate the effects of cer-  
310 tain stratigraphic features on the large-scale microwave emission.

### 311 **3.2.1. Depth hoar**

312 Depth hoar is mostly formed in snowpacks with strong temperature gradients. Its  
313 characteristics include large snow crystals and relatively lower density (mechanically weak  
314 layers), with depth hoar crystal growth depending directly on increased vapor diffusion.  
315 Microwave brightness temperature should be lower for snowpacks with increased snow  
316 grain sizes [*Chang et al., 1982*], since this allows for greater radiative scattering, especially

317 when crystals are of equivalent size to the wavelength. The larger crystals of depth hoar  
318 layers cause a decrease in brightness temperatures relative to snowpacks where such layers  
319 don't exist. In order to demonstrate this effect, we examine the snowpack stratigraphy at  
320 two sites with similar snow accumulation, and the respective satellite observations. Figs  
321 6a-c show snow density, grain size and temperature profiles for the IC12 site, with the  
322 measurement taken on 4 April 2002 and snow depth of 56 cm. Depth hoar was prevalent  
323 in this snowpack, as in other measurement sites across a distance of 15 km shown in Fig.  
324 6e with hoar fraction ranging from 60 to 80%. Measurements at those sites were taken  
325 between 15-17 April 2002, with snow similar depths being similar (coefficient of variation  
326 0.18). The satellite observations for 18.7 and 36.5 GHz (both polarizations, Fig. 6d)  
327 appear very consistent (with only 2 of the sites in the same SSM/I pixel) suggesting that  
328 the effective snowpack properties observed by SSM/I across the 15 km were quite similar.  
329 The stratigraphic profile at the CB04 site (Figs 6f-h) shows that snow crystals are much  
330 smaller than at the IC12 site, while the density profile is similar except for two thin ice  
331 layers near the bottom. Snow depth at the site was 56 cm, with the spatial variability  
332 from two sites within a 15 km distance relatively small (coefficient of variation: 0.14). All  
333 measurements were taken on 28-29 March 2002 (Fig. 6j). SSM/I brightness temperatures  
334 are relatively consistent across these sites (Fig. 6i), and they are higher than the ones for  
335 the depth hoar sites. The differences were about 40 K for both polarizations at 36.5 GHz  
336 (42.7 and 43.2 K for horizontal and vertical respectively), while the respective differences  
337 for 18.7 GHz were smaller (24.0 and 14.5 K). An interesting feature becomes evident when  
338 we examine the microwave emissivity of the site at  $\sim 5$  km from site CB04, which is lower  
339 than the other sites at both frequencies. This discrepancy could be attributed to the

340 slightly higher depth (61 versus 56 cm), but it can also be argued that the larger depth  
341 hoar fraction for that site caused that decrease in brightness temperature. Nonetheless,  
342 the effect of depth hoar on the microwave emission, even at large scales, has been well  
343 known [*Hall et al.*, 1986; *Foster et al.*, 2005] and is also verified by the SnowSTAR 2002-  
344 SSM/I measurements.

### 345 **3.2.2. Inter-layer variability**

346 Two sites with similar snow depths were selected to examine the effects of the density  
347 vertical variability on the large scale microwave emission observed by the satellite. Snow  
348 depth at site ARM was 40 cm, and the observed stratigraphy displays sharp changes in  
349 density with depth (Fig. 7a), while grain size (Fig. 7b) and temperature (Fig. 7c) show  
350 a more typical profile for an Arctic Alaska snowpack. Measurements were taken at three  
351 more sites within a distance of 25 km from ARM on 25, 27, 28 April and 2 May 2002. The  
352 spatial variability in snow depth was relatively high (coefficient of variation 0.46), but the  
353 sites shown are in different SSM/I pixels from ARM. The higher spatial variability is also  
354 evident in the layer fractions (Fig. 7e), where ARM has 50% depth hoar, while the site at  
355 Chukchi (3 km distance) has a much shallower snowpack (11 cm) and a large fraction of  
356 slab (81%, probably caused by local wind effects), and the other two sites have comparable  
357 snow depths (25 and 29 cm) with somewhat smaller depth hoar fractions. The differences  
358 in the stratigraphy between these sites is arguably evident when looking at the SSM/I  
359 observations (Fig. 7d, higher  $T_B$  for lower depths and smaller hoar fractions). Figs 7f,g,h  
360 show density, grain size and depth for the SA03 site, where snow depth was 44 cm and  
361 the density profile is “smoother” than ARM with the exception of a thin slab layer near  
362 the top and a basal ice layer. The sites at a distance of 25 km from SA03 (measurements

363 taken 4-6 April 2002) have similar snow depths (35 and 32 cm) as well as layer fractions  
364 with depth hoar prevalent (Fig. 7j). The brightness temperatures along this transect  
365 (Fig. 7i) range within 7 K for 36.5 GHz, and 3 and 6 K for 18.7 GHz, which can be  
366 attributed to the difference in snow depth between SA03 and the other two sites. When  
367 compared to the ARM site's microwave signature, the feature that stands out is the much  
368 smaller polarization difference for both frequencies (12.9 and 26.1 K at 36.5 GHz and 18.0  
369 and 32.9 K at 18.7 GHz for SA03 and ARM respectively). The layering differences in  
370 the ARM snowpack increases reflection (at layer interfaces), reducing horizontal  $T_{BS}$  and  
371 increasing the polarization difference [Mätzler, 1987; Mätzler and Hüppi, 1989].

### 372 3.2.3. Refrozen snow

373 The microwave signature of melting snow changes dramatically [Tedesco *et al.*, 2006]  
374 raising the emissivity because of increased absorption. When snow refreezes scattering is  
375 increased because of larger effective grain sizes compared to dry snow, while polarization  
376 differences (vertical minus horizontal) become smaller [Choudhury, 1995]. Although re-  
377 frozen snow layers were found in the SnowSTAR 2002 transect measurements and sites  
378 with consistent microwave signatures were found, there were sites with refrozen layers that  
379 did not exhibit the expected behavior. This might be related to horizontal discontinuities  
380 in the refrozen layers within each 25 km pixel affecting the aggregate microwave emission.

### 381 3.2.4. Hydrologic simulations

382 The accuracy of modeling predictions of snow mass and properties depends to a large  
383 degree on the meteorological forcings (e.g. precipitation and air temperature). In-situ  
384 measurement networks of meteorological variables are quite sparse, both spatially and  
385 temporally, while satellite-observed or model-derived meteorological data sets can have

386 large uncertainties [*Adam and Lettenmaier, 2003*] and even large differences between data  
387 sets [*Adler et al., 2001*]. A first assessment of the information content of passive microwave  
388 satellite observations in terms of errors in meteorological forcings that propagate to the  
389 model predictions of snow mass, can be made by comparing the model-predicted  $T_B$  with  
390 the actual satellite observations. Snow hydrologic simulations were performed along the  
391 SnowSTAR 2002 transect with both the 1 and 5-layer VIC models. The required daily  
392 meteorological forcings (precipitation, air temperature and wind speed) were provided  
393 by the ERA-40 re-analysis of meteorological observations globally, including conventional  
394 and satellite measurements and atmospheric model predictions [*Uppala et al., 2005*]. The  
395 SYMAP algorithm [*Shepard, 1984*] was used to interpolate the data from the ERA-40  
396 spatial resolution of  $\sim 1.125$  degrees to the measurement locations.

397 Simulated SWE was overestimated across the transect, shown in Fig. 8 with an estima-  
398 tion error of 89.3 mm. This discrepancy can be attributed to the ERA-40 precipitation  
399 being overestimated and in fact comparisons with in-situ observations from the SNOTEL  
400 network showed large differences in cumulative precipitation [*Shi et al., 2009*]. On the  
401 other hand, daily maximum and minimum air temperatures from ERA-40 showed rela-  
402 tively good agreement with SNOTEL measurements. SWE simulations between the 1 and  
403 5-layer models were almost identical, but the snow depth estimates were different (due  
404 to differences in predicted snow density) although both were higher than the observed  
405 depths (RMSE of 43.7 cm for the 5-layer model).

406 The corresponding simulated  $T_B$  from both the single and multi-layer models along with  
407 the SSM/I observations at the SnowSTAR 2002 transect measurement locations are shown  
408 in Fig. 9. The 1-layer  $T_B$  predictions are consistently higher than the satellite observa-

409 tions for 18.7 GHz (Fig. 9a), despite the fact that simulated snow depths were also higher  
410 than the ones observed. Generally, it would be expected that  $T_B$  would decrease with  
411 increasing depth, but the single-layer model cannot predict the larger depth hoar crystals,  
412 underestimating grain size. The smaller grain size increases  $T_B$ , offsetting the decrease  
413 of  $T_B$  because of the higher snow depth. If the SSM/I radiance observations were assimi-  
414 lated into the single-layer model, predicted SWE (or snow depth) would theoretically be  
415 increased to accommodate the negative difference between the observed and the model-  
416 predicted  $T_B$ . On the other hand, the 5-layer VIC is able to reproduce the larger grain  
417 sizes and predict the lower  $T_B$  relative to the SSM/I observations. Assimilating the latter  
418 into the 5-layer model would theoretically lead to a decrease in snow depth and SWE.  
419 Clearly an actual data assimilation experiment would be needed to correctly evaluate the  
420 analysis SWE and depth estimates, but the innovations (actual minus model-predicted  
421 observations) do provide insight into the potential impact of the assimilation.

422 The 36.5 GHz  $T_B$  simulations (Fig. 9b) exhibited the same qualitative behavior as  
423 the 18.7 GHz. The 1-layer model generally over-predicted  $T_B$ , while the 5-layer model  
424 predicted lower microwave emissivities consistent with the simulated larger snow mass.  $T_B$   
425 predicted by the 5-layer model at the measurement sites at distances from Nome between  
426 600 and 700 km are higher than the observed ones, despite SWE being higher as well.  
427 This is mostly attributable to the underestimation of grain sizes at the mid to upper parts  
428 of the snowpack, leading to an increase in simulated  $T_B$  for 36.5 GHz and not 18.7 GHz  
429 suggesting that depth hoar is reproduced by the model. This highlights the difficulties in  
430 consistently predicting  $T_B$  despite the improvement in the forward models, as well as the

431 relatively large sensitivity to snow grain size, which needs to be taken into account when  
432 assimilating microwave radiances by defining the appropriate uncertainties for it.

#### 4. Conclusions

433 A multilayer snow model was incorporated into a macroscale hydrology model that is  
434 able to account for the effects of topography and vegetation on snow accumulation and  
435 ablation. Snow temperature, density and grain size profiles were reproduced reasonably  
436 well by the model when evaluated with point measurements and using meteorological  
437 forcings that would generally be available for large-scale basin simulations. Improvements  
438 were also shown in predicting microwave brightness temperatures in terms of both absolute  
439 value and frequency/polarization differences when compared with in-situ measurements  
440 from a ground radiometer. Measurements from a snowpit transect across Alaska were  
441 used to examine the effects of stratigraphy on SSM/I satellite observations. Sites with  
442 depth hoar and inter-layer variability exhibited very different passive microwave emission  
443 signatures when compared with sites of comparable snow depth. These effects were evident  
444 across 15-25 km, in agreement with a previous study [*Sturm and Benson, 2004*] that  
445 showed snow layers remaining recognizable over long distances. Because of unavailability  
446 of meteorological forcings along the transect, the ERA-40 re-analysis data set was used  
447 to simulate snow properties and microwave radiances thereafter. The multi-layer coupled  
448 model provided simulations with the expected behavior of lower brightness temperatures  
449 for overestimated snow depth, in contrast with the single-layer model simulations, offering  
450 insight into the potential use as the forward model in a data assimilation system.

451 The lower relief at the satellite scales and the sparse forest cover in Alaska are ideal  
452 for evaluating the passive microwave observations. However in other areas where snow

453 is of key significance to water resources (such as the western U.S.), complex topography,  
454 dense forest cover, and higher spatial variability in snow properties will impede estimation  
455 from data assimilation. Future work should perform data assimilation experiments using  
456 single- and multi-layer models to evaluate the information content of passive microwave  
457 satellite observations, and to identify the optimal model configurations for such a system  
458 (e.g. number of model layers, errors in precipitation, grain size). Although improvements  
459 in snow mass estimates may be incremental and dependent on a number of factors, it  
460 is important to explore and develop approaches to incorporate and digest the long-term  
461 satellite data set, especially for regions where not only in-situ measurements of snow prop-  
462 erties are essentially non-existent, but meteorological forcings for hydrological models are  
463 uncertain.

464 **Acknowledgments.** The authors would like to thank Leung Tsang and Ding Liang for  
465 providing the DMRT code, Matthew Sturm and Glen Liston for making the SnowSTAR  
466 2002 data available, as well as Marco Tedesco for valuable insight during the preparation  
467 of this manuscript.

## References

- 468 Adam, J., and D. Lettenmaier (2003), Adjustment of global gridded precipitation for  
469 systematic bias, *J. Geophys. Res.*, *108*, 4257.
- 470 Adler, R., C. Kidd, G. Petty, M. Morissey, and H. Goodman (2001), Intercomparison  
471 of Global Precipitation Products: The Third Precipitation Intercomparison Project  
472 (PIP-3), *Bull. Amer. Meteorol. Soc.*, *82*(7), 1377–1396.

- 473 Anderson, E. (1976), A point energy and mass balance model of a snow cover, *Tech. Rep.*  
474 *NWS 19*, NOAA.
- 475 Andreadis, K. M., D. Liang, L. Tsang, D. P. Lettenmaier, and E. G. Josberger (2008a),  
476 Characterization of errors in a coupled snow hydrology-microwave emission model, *J.*  
477 *Hydrometeorol.*, *9*, 149–164.
- 478 Andreadis, K. M., P. Storck, and D. P. Lettenmaier (2008b), Modeling snow accumulation  
479 and ablation processes in forested environments, *Water Resour. Res.*, in press.
- 480 Bartelt, P., and M. Lehning (2002), A physical SNOWPACK model for the Swiss avalanche  
481 warning Part I: numerical model, *Cold Reg. Sci. Technol.*, *35*(3), 123–145.
- 482 Boone, A., and P. Etchevers (2001), An Intercomparison of Three Snow Schemes of Vary-  
483 ing Complexity Coupled to the Same Land Surface Model: Local-Scale Evaluation at  
484 an Alpine Site, *J. Hydrometeorol.*, *2*(4), 374–394.
- 485 Bowling, L. C., J. W. Pomeroy, and D. P. Lettenmaier (2004), Parameterization of  
486 Blowing-Snow Sublimation in a Macroscale Hydrology Model, *J. Hydrometeorol.*, *5*(5),  
487 745–762.
- 488 Brun, E. (1989), Investigation on wet-snow metamorphism in respect of liquid-water con-  
489 tent, *Ann. Glaciol.*, *13*, 22–26.
- 490 Brun, E., E. Martin, V. Simon, C. Gendre, and C. Coléou (1989), An energy and mass  
491 model of snow cover suitable for operational avalanche forecasting, *J. Glaciol.*, *35*(121),  
492 333–342.
- 493 Chang, A., J. Foster, D. Hall, A. Rango, and B. Hartline (1982), Snow water equivalent  
494 estimation by microwave radiometry, *Cold Reg. Sci. Technol.*, *5*(3), 259–267.

- 495 Chang, A., J. Foster, and D. Hall (1987), Nimbus-7 SMMR derived global snow cover  
496 parameters, *Ann. Glaciol.*, *9*, 39–44.
- 497 Cherkauer, K. A., and D. P. Lettenmaier (2003), Simulation of spatial variability in snow  
498 and frozen soil, *J. Geophys. Res.*, *108*(D22).
- 499 Choudhury, B. (1995), *Passive Microwave Remote Sensing of Land–Atmosphere Interac-*  
500 *tions*, 228–230 pp., Vsp.
- 501 Cohen, J., and D. Entekhabi (1999), Eurasian snow cover variability and northern hemi-  
502 sphere climate predictability, *Geophys. Res. Lett.*, *26*, 345–348.
- 503 Colbeck, S. (1991), The layered character of snow covers, *Rev. Geophys.*, *29*(1), 81–96.
- 504 Colbeck, S. (1993), The Vapor Diffusion Coefficient for Snow, *Water Resour. Res.*, *29*,  
505 109–109.
- 506 Dennis, J., and R. Schnable (1983), *Numerical methods for unconstrained optimization*  
507 *and nonlinear equations*, Prentice-Hall.
- 508 Derksen, C., A. Walker, and B. Goodison (2003), A comparison of 18 winter seasons  
509 of in situ and passive microwave-derived snow water equivalent estimates in Western  
510 Canada., *Remote Sens. Environ.*, *88*(3), 271–282.
- 511 Derksen, C., A. Walker, and B. Goodison (2005), Evaluation of passive microwave snow  
512 water equivalent retrievals across the boreal forest/tundra transition of western Canada,  
513 *Remote Sens. Environ.*, *96*(3-4), 315–327.
- 514 Dong, J., J. Walker, and P. Houser (2005), Factors affecting remotely sensed snow water  
515 equivalent uncertainty, *Remote Sens. Environ.*, *97*(1), 68–82.
- 516 Duguay, C., J. Green, C. Derksen, M. English, A. Rees, M. Sturm, and A. Walker (2005),  
517 Preliminary assessment of the impact of lakes on passive microwave snow retrieval al-

518 algorithms in the Arctic, in *Proc 62nd Eastern Snow Conference, Waterloo, Ontario*, pp.  
519 223–228.

520 Durand, M., and S. Margulis (2006), Feasibility test of multifrequency radiometric data  
521 assimilation to estimate snow water equivalent, *J. Hydrometeorol.*, 7(3), 443–457.

522 Durand, M., E. Kim, and S. Margulis (2008), Quantifying Uncertainty in Modeling Snow  
523 Microwave Radiance for a Mountain Snowpack at the Point-Scale, Including Strati-  
524 graphic Effects, *IEEE Trans. Geosci. Remote Sens.*, 46(6), 1753–1767.

525 Edgerton, A., A. Stogryn, and G. Poe (1971), Microwave radiometric investigations of  
526 snowpacks, *Aerojet Gen. Corp., Microwave Div., El Monte, CA, Final Rep.*

527 Etchevers, P., et al. (2004), Validation of the energy budget of an alpine snowpack simu-  
528 lated by several snow models (SnowMIP project), *Ann. Glaciol.*, 38(1), 150–158.

529 Foster, J., C. Sun, J. Walker, R. Kelly, A. Chang, J. Dong, and H. Powell (2005), Quanti-  
530 fying the uncertainty in passive microwave snow water equivalent observations, *Remote*  
531 *Sens. Environ.*, 94(2), 187–203.

532 Graf, T., T. Koike, H. Fujii, M. Brodzik, and R. Armstrong (2003), CLPX-Ground:  
533 Ground Based Passive Microwave Radiometer (GBMR-7) Data, *Boulder, CO: National*  
534 *Snow and Ice Data Center. Digital Media.*

535 Grody, N., and A. Basist (1996), Global identification of snowcover using SSM/I mea-  
536 surements, *IEEE Trans. Geosci. Remote Sens.*, 34(1), 237–249.

537 Hall, D., A. Chang, and J. Foster (1986), Detection of the depth-hoar layer in the snow-  
538 pack of the Arctic Coastal Plain of Alaska, USA, using satellite data, *J. Glaciol.*,  
539 32(110), 87–94.

- 540 Hallikainen, M., and P. Jolma (1992), Comparison of algorithms for retrieval of snow  
541 water equivalent from Nimbus-7 SMMR data in Finland, *IEEE Trans. Geosci. Remote*  
542 *Sens.*, *30*(1), 124–131.
- 543 Heim, R., and K. F. Dewey (1984), Circulation patterns and temperature fields associated  
544 with extensive snow cover on the north american continent, *Phys. Geogr.*, *4*, 66–85.
- 545 Hofer, R., and C. Mätzler (1980), Investigations on snow parameters by radiometry in the  
546 3-to 60-mm wavelength region, *J. Geophys. Res.*, *85*(C1), 453–460.
- 547 Jin, J., X. Gao, S. Sorooshian, Z. Yang, R. Bales, R. Dickinson, S. Sun, and G. Wu (1999),  
548 One-dimensional snow water and energy balance model for vegetated surfaces, *Hydrol.*  
549 *Process.*, *13*, 2467–2482.
- 550 Jordan, R. (1991), A one-dimensional temperature model for a snowcover: technical doc-  
551 umentation for sntherm. 89, *Tech. rep.*, US Army Cold Regions Res. Engrg. Lab.,  
552 Hanover, NH.
- 553 Josberger, E., and N. Mognard (2002), A passive microwave snow depth algorithm with  
554 a proxy for snow metamorphism, *Hydrol. Process.*, *16*(8), 1557–1568.
- 555 Kelly, R., A. Chang, L. Tsang, and J. Foster (2003), A prototype AMSR-E global snow  
556 area and snow depth algorithm, *IEEE Trans. Geosci. Remote Sens.*, *41*(2), 230–242.
- 557 Koren, V., J. Schaake, K. Mitchell, Q. Duan, F. Chen, and J. Baker (1999), A Parame-  
558 terization of Snowpack and Frozen Ground intended for NCEP Weather and Climate  
559 Models, *J. Geophys. Res.*, *104*(D16), 19–569.
- 560 Künzi, K., S. Patil, and H. Rott (1982), Snow-Cover Parameters Retrieved from Nimbus-  
561 7 Scanning Multichannel Microwave Radiometer (SMMR) Data, *IEEE Trans. Geosci.*  
562 *Remote Sens.*, pp. 452–467.

- 563 Lehning, M., P. Bartelt, B. Brown, C. Fierz, and P. Satyawali (2002), A physical SNOW-  
564 PACK model for the Swiss avalanche warning Part II. Snow microstructure, *Cold Reg.*  
565 *Sci. Technol.*, *35*(3), 147–167.
- 566 Liang, D., X. Xu, L. Tsang, K. Andreadis, and E. Josberger (2008), The Effects of Layers  
567 in Dry Snow on Its Passive Microwave Emissions Using Dense Media Radiative Trans-  
568 fer Theory Based on the Quasicrystalline Approximation (QCA/DMRT), *IEEE Trans.*  
569 *Geosci. Remote Sens.*, *46*(11), 3663.
- 570 Liang, X., D. P. Lettenmaier, E. F. Wood, and S. J. Burges (1994), A simple hydrologically  
571 based model of land surface water and energy fluxes for general circulation models, *J.*  
572 *Geophys. Res.*, *99*(14), 415–14.
- 573 Loth, B., H. Graf, and J. Oberhuber (1993), Snow cover model for global climate simula-  
574 tions, *J. Geophys. Res.*, *98*(D6), 10,451–10,464.
- 575 Mätzler, C. (1987), *Applications of the Interaction of Microwaves with the Natural Snow*  
576 *Cover*, Harwood Academic Publishers.
- 577 Mätzler, C., and R. Hüppi (1989), Review of signature studies for microwave remote  
578 sensing of snowpacks, *Adv. Space Res.*, *9*(1), 253–265.
- 579 Maurer, E., A. Wood, J. Adam, D. Lettenmaier, and B. Nijssen (2002), A long-term  
580 hydrologically based dataset of land surface fluxes and states for the conterminous  
581 United States, *J. Climate*, *15*(22), 3237–3251.
- 582 Pulliainen, J. (2006), Mapping of snow water equivalent and snow depth in boreal and sub-  
583 arctic zones by assimilating space-borne microwave radiometer data and ground-based  
584 observations, *Remote Sens. Environ.*, *101*(2), 257–269.

- 585 Rosenfeld, S., and N. Grody (2000a), Anomalous microwave spectra of snow cover  
586 observed from Special Sensor Microwave/Imager measurements, *J. Geophys. Res.*,  
587 *105*(D11), 14,913–14,926.
- 588 Rosenfeld, S., and N. Grody (2000b), Metamorphic signature of snow revealed in SSM/I  
589 measurements, *IEEE Trans. Geosci. Remote Sens.*, *38*(1), 53–63.
- 590 Schmugge, T. J., W. P. Kustas, J. C. Ritchie, T. J. Jackson, and A. Rango (2002), Remote  
591 sensing in hydrology, *Adv. Water Resour.*, *25*(8-12), 1367–1385.
- 592 Schweizer, J., and K. Kronholm (2007), Snow cover spatial variability at multiple scales:  
593 Characteristics of a layer of buried surface hoar, *Cold Reg. Sci. Technol.*, *47*(3), 207–223.
- 594 Shepard, D. (1984), Computer mapping: The SYMAP interpolation algorithm, in *Spatial*  
595 *Statistics and Models*, edited by G. L. Gaile and C. J. Wilmott, pp. 133–145, Springer.
- 596 Shi, X., M. Sturm, G. E. Liston, R. E. Jordan, and D. P. Lettenmaier (2009), Snow-  
597 STAR2002 transect reconstruction using a multilayered energy and mass balance snow  
598 model, *J. Hydrometeorol.*, in review.
- 599 Sturm, M. (1992), Snow distribution and heat flow in the taiga, *Arct. Alp. Res.*, *24*(2),  
600 145–152.
- 601 Sturm, M., and C. Benson (1997), Vapor transport, grain growth and depth-hoar devel-  
602 opment in the subarctic snow, *J. Glaciol.*, *43*(143), 42–59.
- 603 Sturm, M., and C. Benson (2004), Scales of spatial heterogeneity for perennial and sea-  
604 sonal snow layers, *Ann. Glaciol.*, *38*, 253–260.
- 605 Sturm, M., and G. Liston (2003), The snow cover on lakes of the Arctic Coastal Plain of  
606 Alaska, USA, *J. Glaciol.*, *49*(166).

- 607 Sturm, M., J. Holmgren, M. Koenig, and K. Morris (1997), The thermal conductivity of  
608 seasonal snow, *J. Glaciol.*, *43*(143), 26–41.
- 609 Sun, S., J. Jin, and Y. Xue (1999), A simple snow-atmosphere-soil transfer model, *J.*  
610 *Geophys. Res.*, *104*(D16), 19,587–19,598.
- 611 Tedesco, M., E. Kim, A. England, R. De Roo, and J. Hardy (2006), Brightness Temper-  
612 atures of Snow Melting/Refreezing Cycles: Observations and Modeling Using a Multi-  
613 layer Dense Medium Theory-Based Model, *IEEE Trans. Geosci. Remote Sens.*, *44*(12),  
614 3563–3573.
- 615 Thornton, P., and S. Running (1999), An improved algorithm for estimating incident daily  
616 solar radiation from measurements of temperature, humidity, and precipitation, *Agric.*  
617 *For. Meteorol.*, *93*(4), 211–228.
- 618 Tsang, L., J. Kong, and R. Shin (1985), *Theory of microwave remote sensing*, Wiley.
- 619 Tsang, L., C. Chen, A. Chang, J. Guo, and K. Ding (2000), Dense media radiative transfer  
620 theory based on quasi-crystalline approximation with applications to passive microwave  
621 remote sensing of snow, *Radio Sci.*, *35*, 731–749.
- 622 Tsang, L., J. Pan, D. Liang, Z. X. Li, D. Cline, and Y. H. Tan (2007), Modeling active mi-  
623 crowave remote sensing of snow using Dense Media Radiative Transfer (DMRT) theory  
624 with multiple scattering effects, *IEEE Trans. Geosci. Remote Sens.*, *45*, 990–1004.
- 625 Uppala, S., et al. (2005), The ERA-40 re-analysis, *Quart. J. Roy. Meteorol. Soc.*, *131*,  
626 2961–3012.
- 627 Verseghy, D. L. (1991), CLASS-A Canadian Land Surface Scheme for GCMS: I. Soil  
628 Model, *Int. J. Climatol.*, *11*(2), 111–133.

- 629 Wiesmann, A., and C. Mätzler (1999), Microwave emission model of layered snowpacks,  
630 *Remote Sens. Environ.*, *70*(3), 307–316.
- 631 Wigmosta, M., L. Vail, and D. Lettenmaier (1994), A distributed hydrology-vegetation  
632 model for complex terrain, *Water Resour. Res.*, *30*(6), 1665–1680.
- 633 Yang, Z., R. Dickinson, A. Robock, and K. Vinnikov (1997), Validation of the Snow  
634 Submodel of the Biosphere–Atmosphere Transfer Scheme with Russian Snow Cover  
635 and Meteorological Observational Data, *J. Climate*, *10*(2), 353–373.

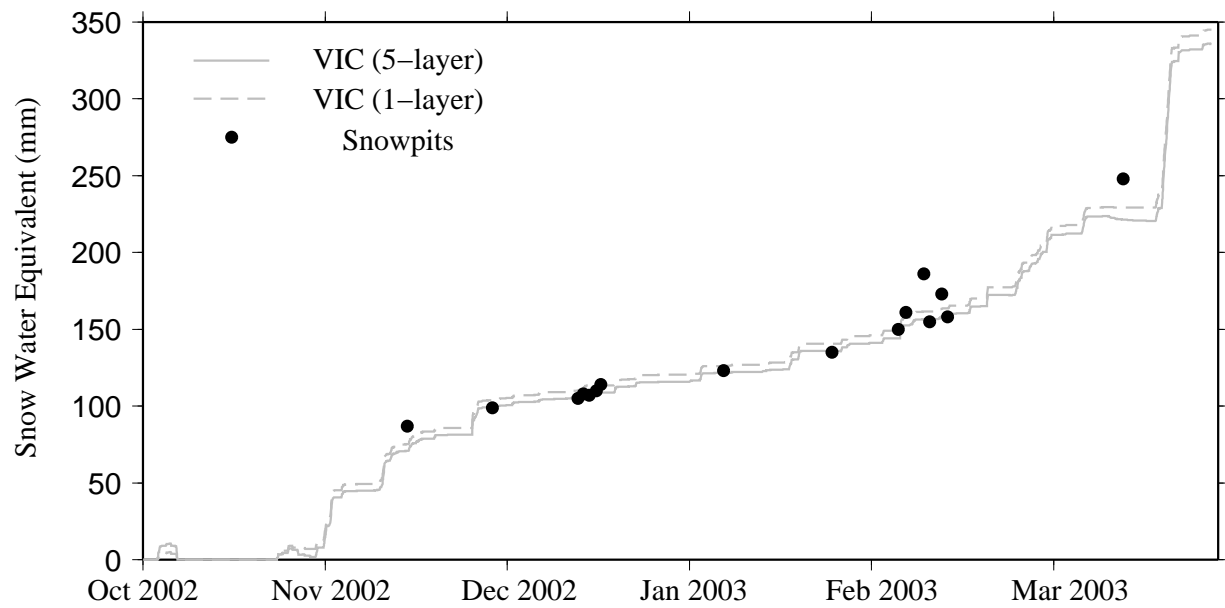


Figure 1: Simulated snow water equivalent for the multiple and single-layer VIC models compared with snowpit measurements from the CLPX Local Scale Observation Site.

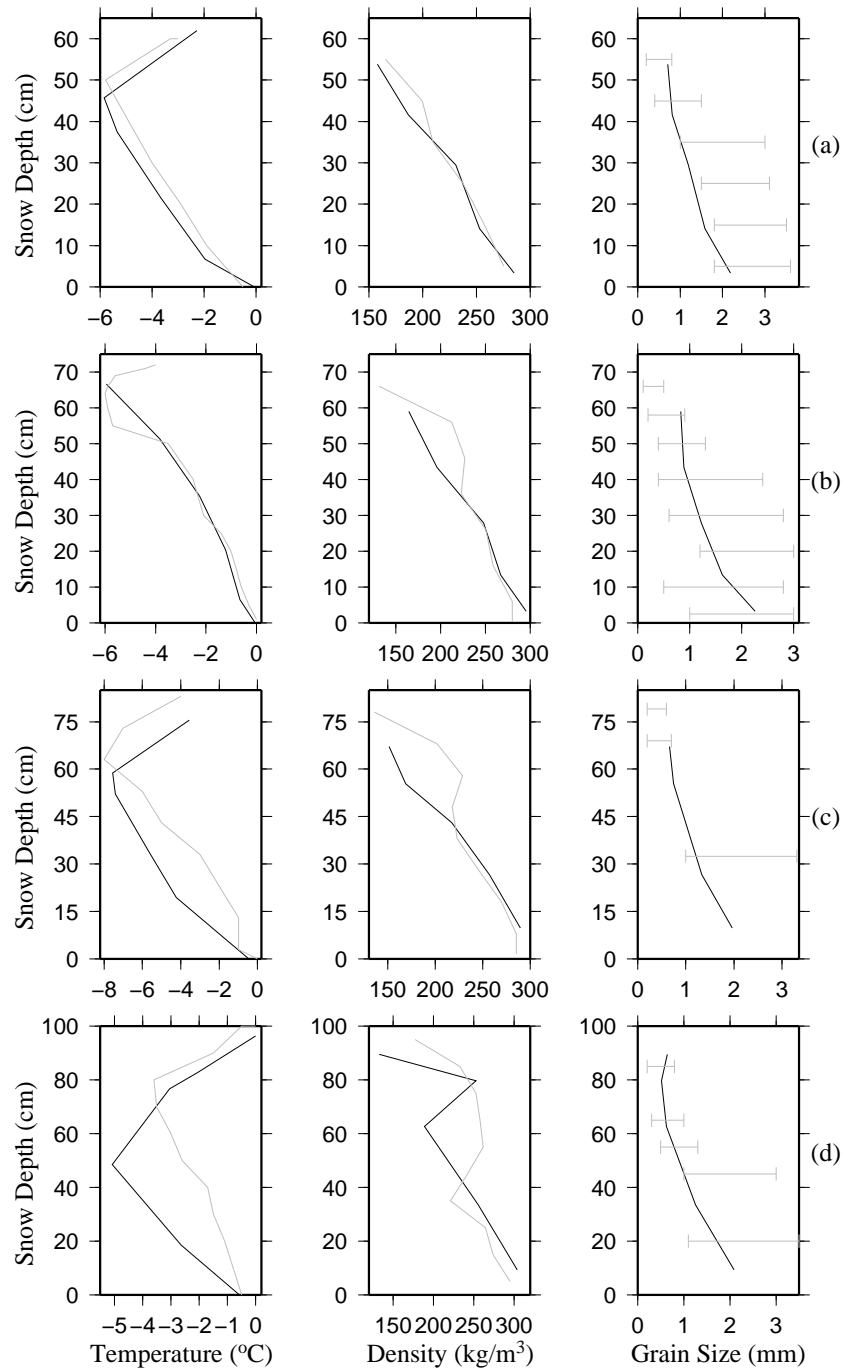


Figure 2: Simulated (black) and observed (gray) snow temperature (left), density (middle), grain size (right) profiles for selected dates, 22 January (a), 3 February (b), 20 February (c) and 11 March 2003 (d), at the CLPX LSOS site, Colorado.

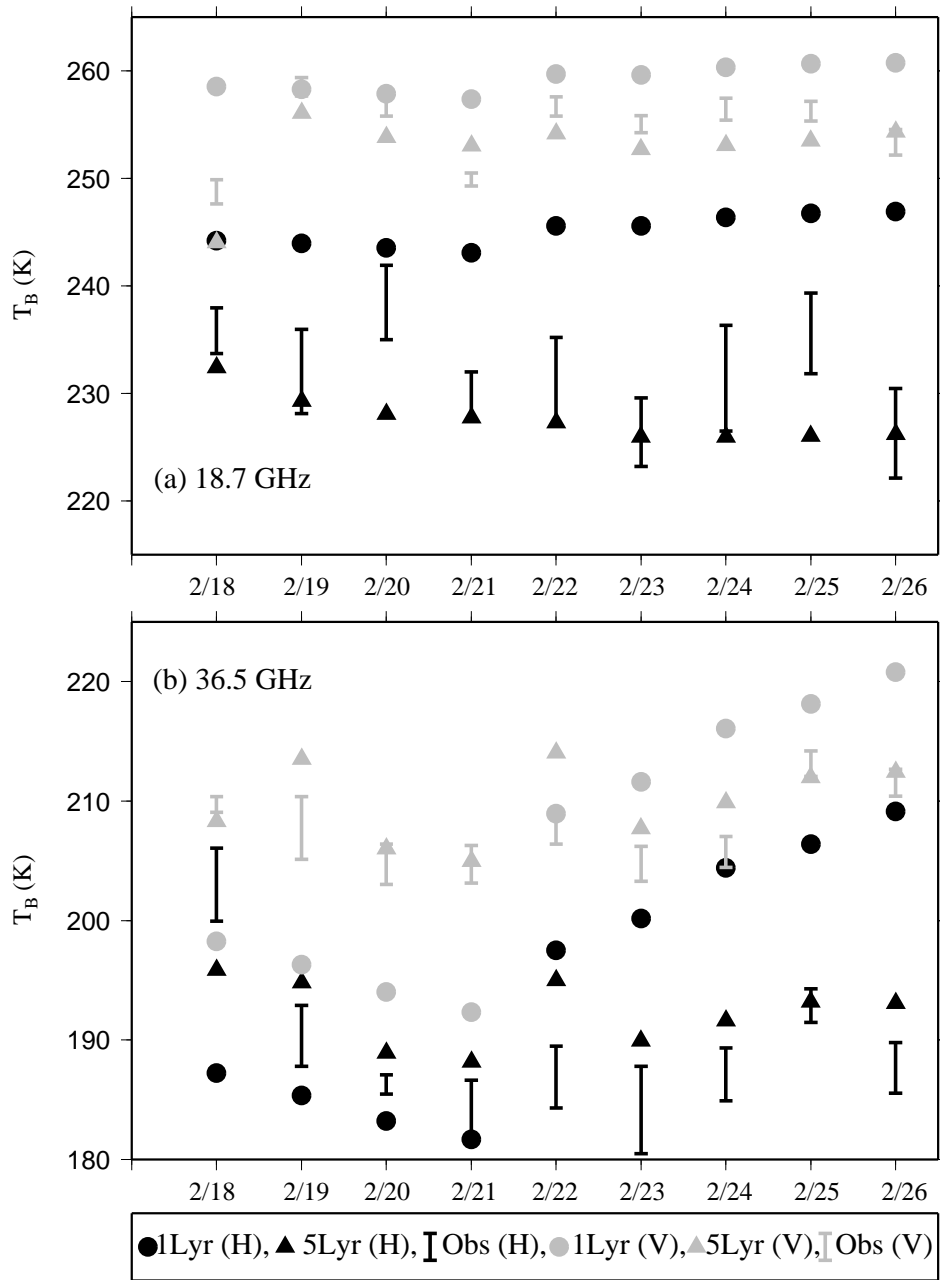


Figure 3: Observed (vertical bars), 1-layer (circles) and 5-layer (triangles) simulated brightness temperatures at horizontal (black) and vertical (grey) polarizations at 18.7 (top panel) and 36.5 (bottom panel) GHz from the CLPX LSOS site, Colorado.

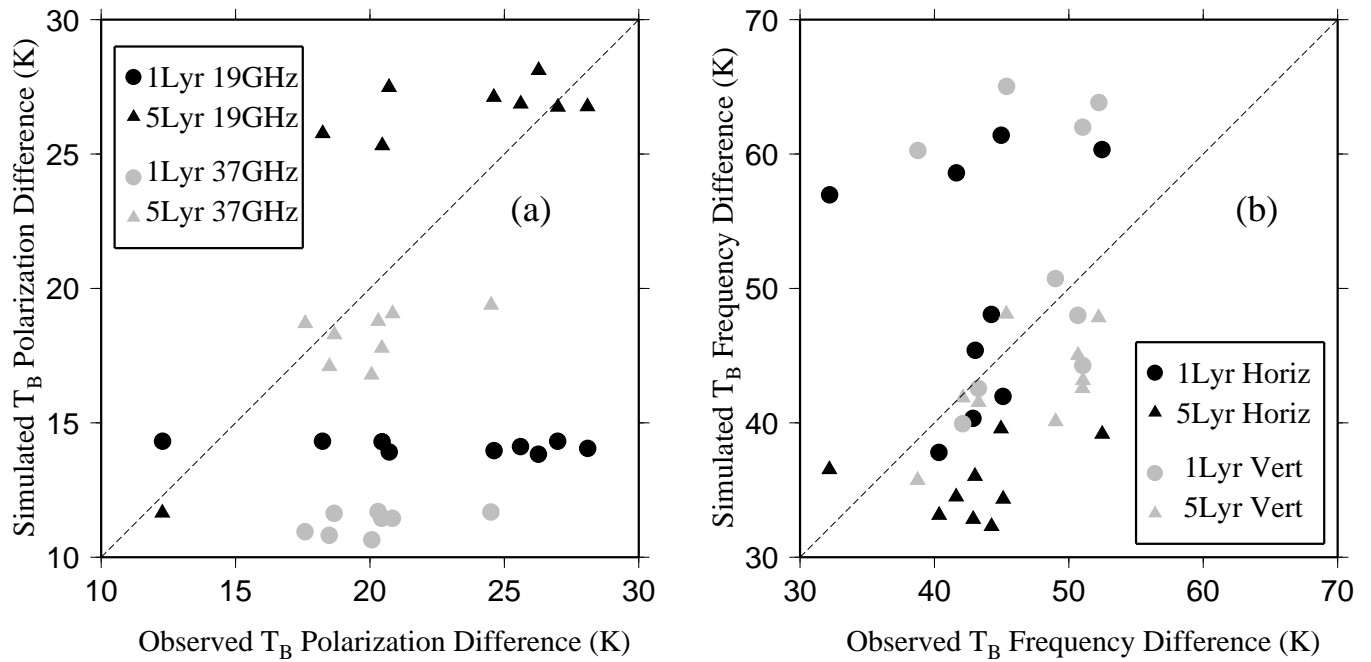


Figure 4: (a) Simulated versus observed brightness temperature polarization differences for the 5-layer (triangles) and 1-layer (circles) models, 18.7 (black) and 36.5 (grey) GHz. (b) Simulated versus observed brightness temperature frequency differences for the 5-layer (triangles) and 1-layer (circles) models, horizontal (black) and vertical (grey) polarizations.

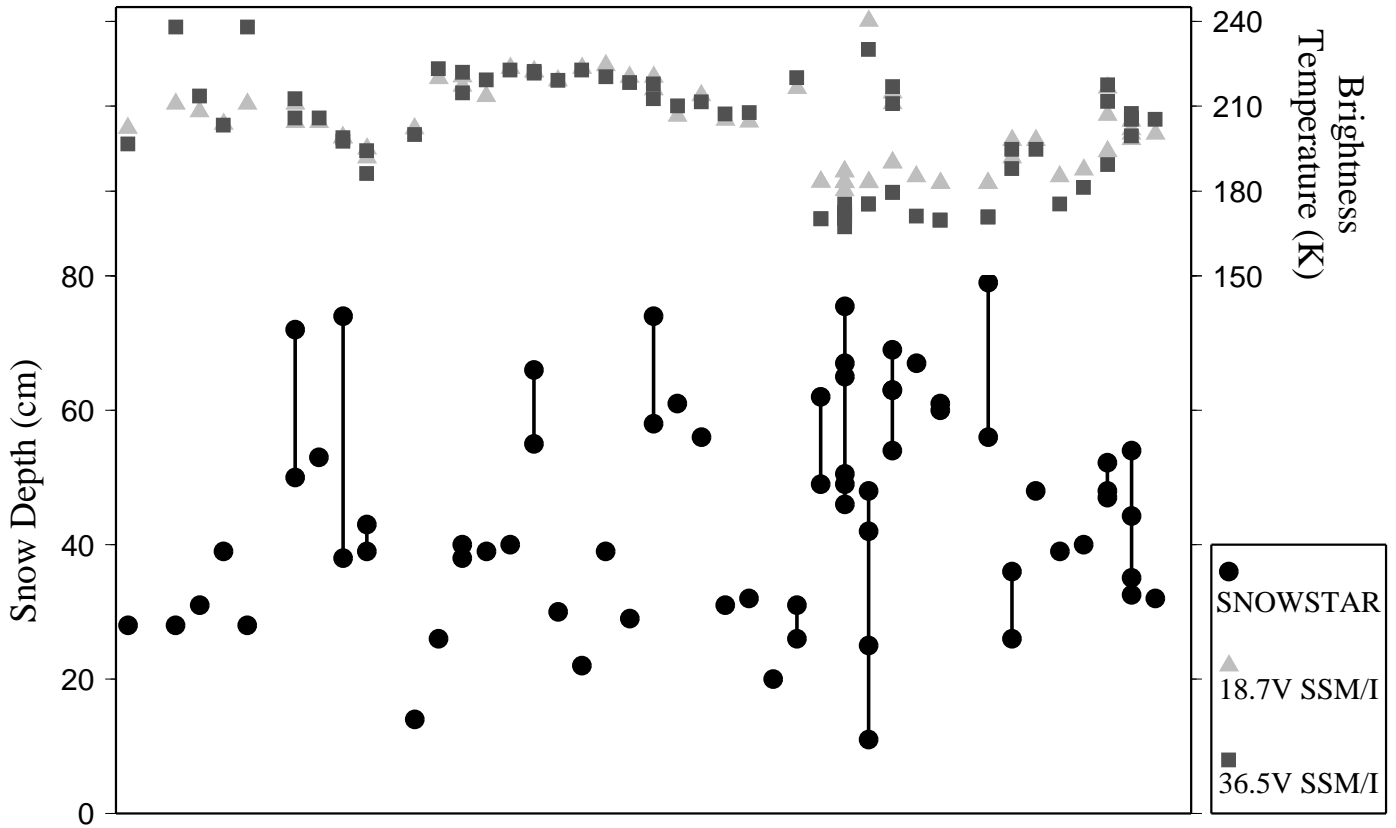


Figure 5: SnowSTAR 2002 transect snow depth (circles) at each co-registered SSM/I 25×25 km pixel and corresponding observed brightness temperature at 37 GHz, vertical (triangles) and horizontal (squares) polarization.

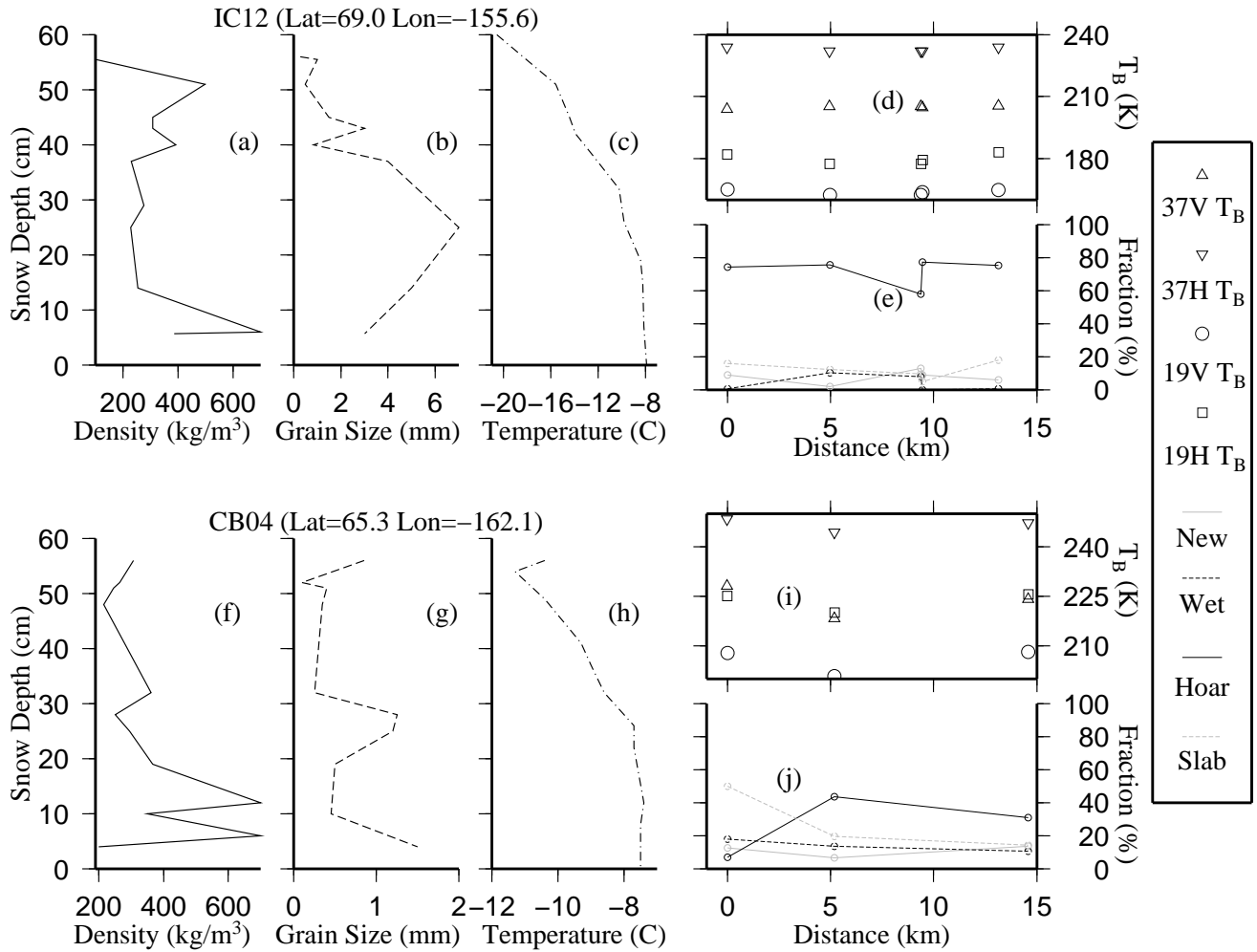


Figure 6: Snowpack stratigraphy profiles (density, grain size, temperature) for two SnowSTAR 2002 sites: IC12 (prevalent depth hoar, (a), (b), and (c)) and CB04 (fine/middle grain, (f), (g), and (h)); SSM/I observed brightness temperatures at measurement sites over 15 km distances from both sites ((d) and (i) respectively) at 18.7 horizontal (triangles), vertical (inverted triangles) and 36.5 GHz horizontal (circles) and vertical (squares); and layer fractions at measurement sites over 15 km distances from both sites ((e) and (j) respectively) with new snow (grey line), wet/icy snow (black dashed line), depth hoar (black line), and slab (grey dashed line) fractions.

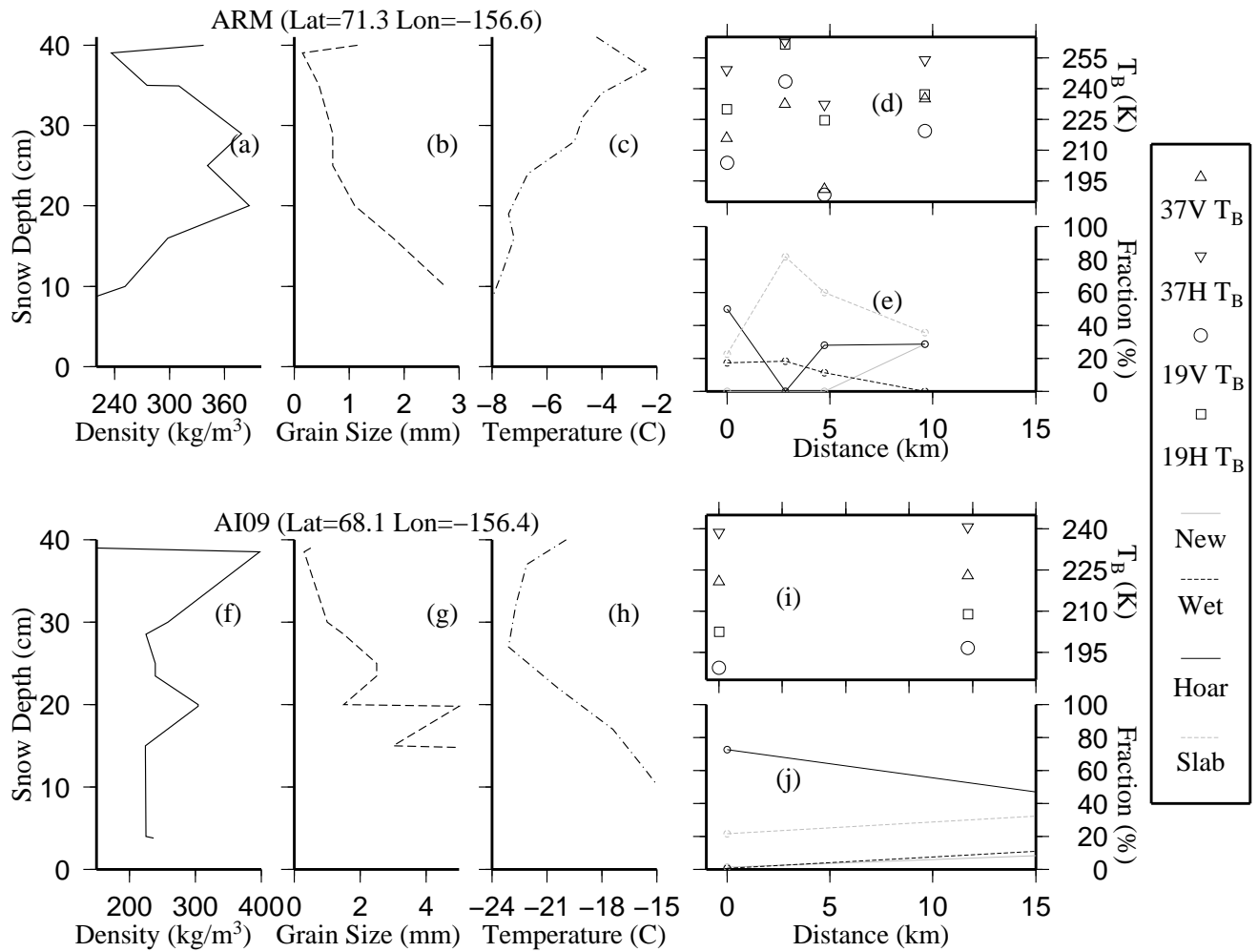


Figure 7: Snowpack stratigraphy profiles (density, grain size, temperature) for two SnowSTAR 2002 sites: ARM (snowpack with large inter-layer density differences, (a), (b), and (c)) and SA03 (mostly depth hoar and slab layers, (f), (g), and (h)); SSM/I observed brightness temperatures at measurement sites over 25 km distances from both sites ((d) and (i) respectively) at 18.7 horizontal (triangles), vertical (inverted triangles) and 36.5 GHz horizontal (circles) and vertical (squares); and layer fractions at measurement sites over 25 km distances from both sites ((e) and (j) respectively) with new snow (grey line), wet/icy snow (black dashed line), depth hoar (black line), and slab (grey dashed line) fractions.

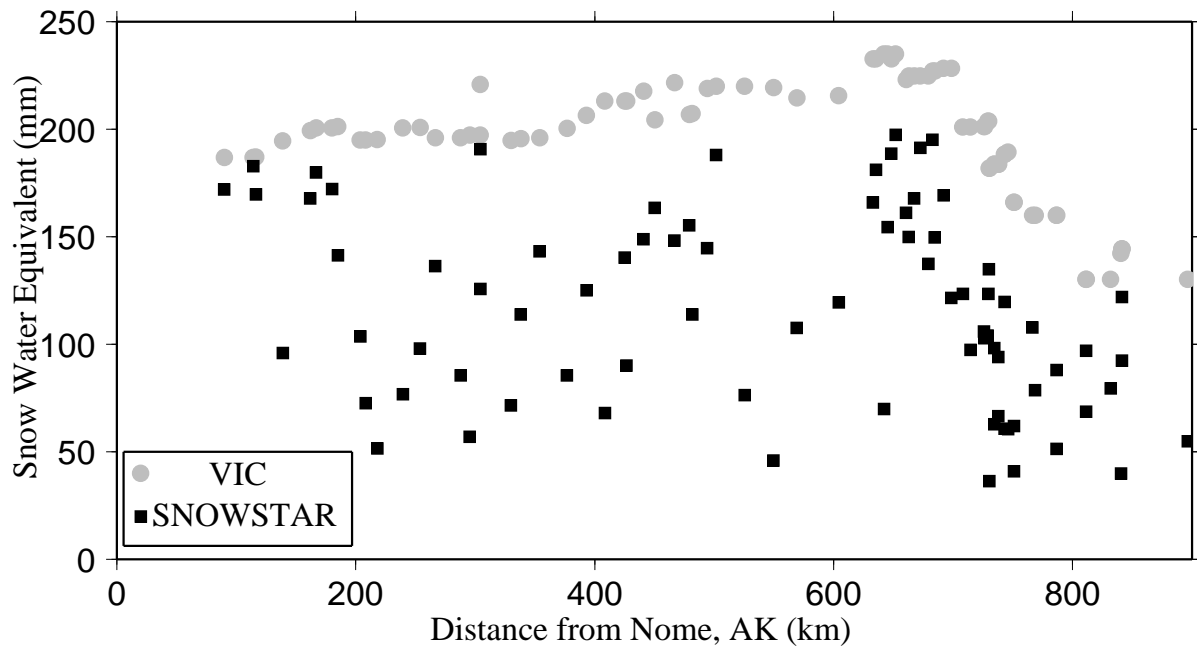


Figure 8: Simulated (grey squares) and observed (black circles) snow water equivalent along the SnowSTAR 2002 transect.

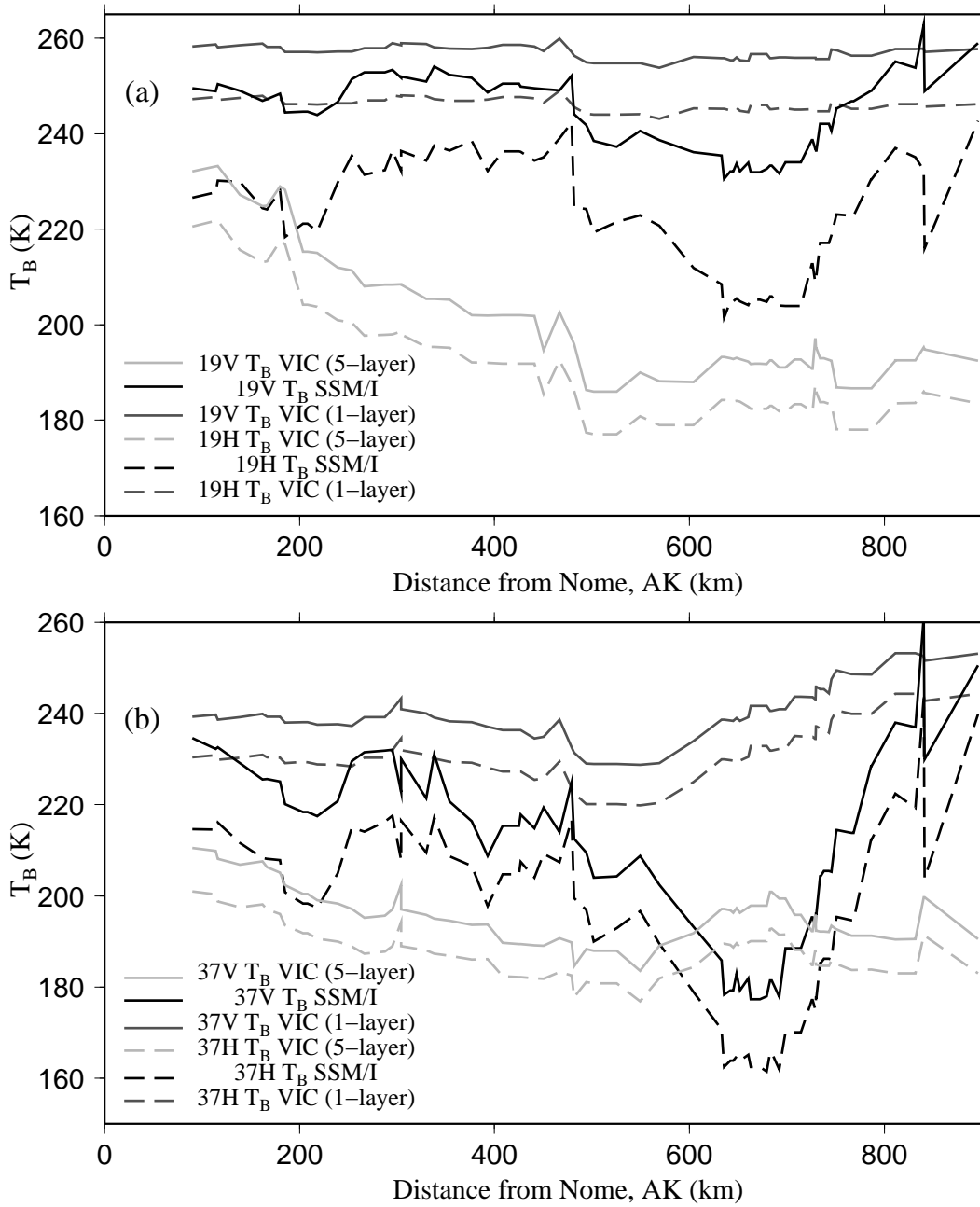


Figure 9: Observed  $T_B$  from SSM/I, and simulated  $T_B$  from the 1 and 5-layer VIC/DMRT along the SnowSTAR 2002 transect for both horizontal and vertical polarizations at 18.7 (a) and 36.5 (b) GHz.